



Spatiotemporal trends of urban-induced land use and land cover change and implications on catchment surface imperviousness

Tesfa Gebrie Andualem^{1,2} · Stefan Peters¹ · Guna A. Hewa¹ · John Boland¹ · Baden R. Myers¹

Received: 27 June 2023 / Accepted: 11 October 2023 / Published online: 4 November 2023
© The Author(s) 2023

Abstract

Urbanization, changes in land use and land cover (LULC), and an increase in population collectively have significant impacts on urban catchments. However, a vast majority of LULC studies have been conducted using readily available satellite imagery, which often presents limitations due to its coarse spatial resolution. Such imagery fails to accurately depict the surface characteristics and diverse spectrum of LULC classifications contained within a single pixel. This study focused on the highly urbanized Dry Creek catchment in Adelaide, South Australia and aimed to determine the impact of urbanization on spatiotemporal changes in LULC and its implications for the land surface condition of the catchment. Very high spatial resolution imagery was utilized to examine changes in LULC over the past four decades. Support Vector Machine-learning-based image classification was utilized to classify and identify the changes in LULC over the study area. The classification accuracy showed strong agreement, with a kappa value greater than 0.8. The findings of this analysis showed that extensive urban development, which expanded the built-up area by 34 km², were responsible for the decline in grass cover by 43.1 km² over the last 40 years (1979–2019). Moreover, built-up areas, plantation, and water features, in contrast to grass cover, have demonstrated an increasing trend during the study period. The overall urban expansion over the study period was 136.6%. Urbanization intensified impervious area coverage, increasing the runoff coefficient, equivalent impervious area, and curve number by 60.6%, 60.6%, and 7.9%, respectively, while decreasing the retention capacity by 38.6%. These modifications suggest a potential variability in catchment surface runoff, prompting the need for further research to understand the surface runoff changes brought by the changes in LULC resulting from urbanization. The findings of this study can be used for land use planning and flood management.

Keywords Change detection, dry creek · Imperviousness · LULC · SVM · Urbanization

Introduction

Population growth and increased migration to urban areas have contributed to have increased urbanization affecting the LULC dynamics of an area (Aburas et al. 2019; Gashu and Gebre-Egziabher 2018; Shawul and Chakma 2019), consequently influencing the quantity of runoff and sediment transport (Bledsoe 2002). Urbanization is a worldwide phenomenon characterized by increasing built-up features and the conversion of natural landscapes for residential,

commercial, and industrial land use activities (Li et al. 2018; Pradhan 2017). Urban sprawl transforms non-urban land into built-up areas (roads, rooftops, parking lots, and other urban surfaces), which significantly increases the proportion of impervious surfaces (Ding et al. 2022; Li et al. 2018) causing considerable flooding and waterlogging in urban catchments (Moniruzzaman et al. 2020). This results in decreased infiltration, higher surface runoff, and flooding in downstream areas (Feng et al. 2021).

The analysis of LULC changes is necessary to determine the extent and magnitude of urban expansion (Grigorescu et al. 2021). Studying changes in LULC is essential for evaluating its environmental impact in terms of both spatial and temporal dimensions (Gashu and Gebre-Egziabher 2018; Shawul and Chakma 2019), including the influence on river discharge and sediment yield. Remote sensing plays an important role in detecting LULC changes (Jamali et al.

✉ Tesfa Gebrie Andualem
andtg003@mymail.unisa.edu.au

¹ UniSA-STEM, University of South Australia, Mawson Lakes, Adelaide, SA 5095, Australia

² Department of Hydraulic and Water Resources Engineering, Debre Tabor University, 272, Debre Tabor, Ethiopia

2022; Jat et al. 2008; Rojas et al. 2013; Sidhu et al. 2018) and their impact on runoff (Demekke and Andualem 2018), sediment yield, and channel morphology. IDRISI Selva (IDRISI), Sentinel Application Platform (SNAP), Earth Resources Data Analysis System (ERDAS Imagine), Environment for Visualizing Images (ENVI), ArcGIS Pro and Google Earth Engine are the most common remote sensing tools used for LULC classification (Jamali et al. 2022; Jat et al. 2008; Sidhu et al. 2018).

Several image classification methods, including the ISO cluster unsupervised classification, Maximum Likelihood (ML), random tree, Support Vector Machine (SVM), and K-nearest neighbor, can be used to produce a LULC map and assess the impact of urbanization (Chandra and Bedi 2021). Unlike unsupervised classification, supervised classification allows the user to select image pixel samples to classify data into groups, such as special subcategories, by providing training samples to cluster new inputs into predefined groups, map features according to their respective groups, and to provide high accuracy (Hu and Dong 2018; Nguyen 2020). The most frequent approach in land use classification and change detection is supervised image classification, which is a user-guided classification utilizing training samples. The most successful technique for detecting changes in land use has been identified as SVM (Kesikoglu et al. 2019). In comparison with other classification techniques, recent studies have demonstrated that supervised image classification using an SVM classifier has the highest accuracy in LULC analysis (Basheer et al. 2022; Dabija et al. 2021; Thanh Noi and Kappas 2017; Xie and Niculescu 2021). The SVM classifier uses statistical learning theory and is an advanced and powerful machine learning classification technique (Chandra and Bedi 2021; Mohammed and Sulaiman 2012). It can handle segmented raster data and common image inputs with less noise susceptibility (Ding et al. 2022; Lamine et al. 2018). In addition, this approach makes use of object-based classification, which involves image segmentation using spatial, spectral, and size information. This approach more closely mimics real-world features and yields more accurate categorization results for high-resolution imageries (Blaschke et al. 2014; Li and Shao 2014; Peña et al. 2014).

The accuracy of LULC change detection studies are dependent on spatial scale or map resolution (Manandhar et al. 2010). LULC change analysis has been conducted in several studies by employing different satellite imagery resolutions. Some studies have utilized a coarse spatial resolution of 250-m from a Moderate Resolution Imaging Spectroradiometer (MODIS) sensor (Yin et al. 2014), and 60 m (Ding et al. 2022); while, others have worked with moderate resolutions of 15 m (Mansour et al. 2020), and 30 m (Hu and Dong 2018; Hussien et al. 2022; Malede et al. 2022; Silva et al. 2018). The spatial resolution of

imagery affects the accuracy of classification and representativeness of the resulting LULC map for the intended purposes (Chen et al. 2004; Fisher et al. 2018). The provision of high-resolution spatial imagery of urban areas (Chen et al. 2004; Zhen et al. 2013) provides an opportunity to clearly identify the pervious and impervious surface conditions of the study area. Unlike coarse resolution pixels (such as 30×30 m), finer resolution pixels (2.5 m and finer) can be utilized to distinguish road, roof, grass, and tree characteristics that can be present within a 30×30 m ground spatial position. Satellite sensors such as Landsat, Sentinel, and/or ASTER have high spectral resolution and multispectral bands such as Red Edge (RE), Near Infrared (NIR), Shortwave Infrared (SWIR), and Thermal Infrared (TIR), which are effective for moisture/water extraction and vegetation health (Amani et al. 2018). Compared to high spectral resolution, their spatial resolution is inadequate for distinguishing various land use aspects that depict surface imperviousness. Therefore, this study employed high-resolution SPOT5 pan-sharpened satellite and aerial imagery to quantify the spatial and temporal extent of LULC change and its implications on the surface imperviousness of a catchment.

It is crucial to manage and mitigate the ecological and geomorphological effects of urban development by comprehending the effects of urbanization on fluvial systems and sedimentation through the analysis of spatiotemporal changes in urbanization (Chin et al. 2013; Ciupa & Suligowski 2020; O'Driscoll et al. 2010). Surface imperviousness is comparatively high in established urban catchments and has been associated with higher runoff and lower levels of total suspended sediment discharge (Myers et al. 2021). Therefore, in recent years, determining how urbanization affects hydrology of the catchment and channel stability has gained significant importance (O'Driscoll et al. 2010).

The Dry creek catchment is an urbanized catchment in the metropolitan area of Adelaide, South Australia, with significant land use changes due to urban sprawl since the 1970s (Wilkinson 2005). These changes have resulted in alterations to the surface imperviousness and hydrological system of the catchment. A recent modeling study focused on the Parafield stormwater harvesting scheme, a part of the Dry Creek catchment, has revealed that urban development within the catchment could potentially result in a 20% increase in impervious area (Clark et al. 2015). However, to date, no research has been undertaken within the catchment to explore the implications of urban-induced LULC changes and their influence on the surface imperviousness of the area. Therefore, this study aimed to examine the long-term spatiotemporal trends of urban-induced LULC change and its implication on surface imperviousness over the urbanized Dry Creek catchment between 1979 and 2019 using very high-resolution multispectral imagery.

Materials and methods

Study area description

This study focused on the Dry Creek catchment, which is located in the Northern part of Adelaide, South Australia. The catchment is located between 138°35'0" and 138°46'0" E longitude and 34°51'18" and 34°45'28" S latitude (Fig. 1). The study area covers about 115.4 km². The inner norther suburbs of Adelaide, which encompass the Dry Creek catchment, were projected to reach a population of 315,367 by 2021 (Department of Planning Transport and Infrastructure 2019a). The topography of the catchment ranges between 0 and 424.81 m AHD (Australian Height Datum). The annual rainfall of the catchment ranges between 450 and 700 mm (The Goyder Institute for Water Research 2016).

In contrast to the upper watershed, which is primarily rural, the lower catchment is primarily dense residential, commercial, and industrial, and contains some salt fields scheduled for development and various constructed wetlands. According to the Department of Planning, Transport and Infrastructure (DPTI) (Department of Planning Transport and Infrastructure 2017), the 30-year plan for Greater Adelaide showed that the Dry Creek catchment area has been marked as a potential urban growth area.

The increase in urban growth rises the impervious surface area with a potential of flooding to the downstream environment.

Data source

Very high-resolution aerial imagery (1979 and 2019) and SPOT imagery (2006) were obtained from the South Australian Department for Environment and Water (DEW) and used to identify the various LULC types found throughout the catchment (Table 1). The study period was chosen based on the availability of very high-resolution imagery encompassing the entire catchment, as well as the period when the population began to grow, potentially resulting in urban expansion. The higher resolution (0.075 m and 0.25 m) imagery was resampled using the nearest neighbor resampling technique to a lower resolution (2.5 m) prior to undertaking the classification to make change detection simple. The data were pre-processed (resampling and segmentation) and used in the ArcGIS Pro 3.0 environment to create LULC maps.

Although raster imagery with smaller cell sizes results in a larger file size and takes longer to process, its importance in LULC classification cannot be overstated. This is due to its higher spatial resolution, which provides finer details of land surface features. The hydrologic soil group of the area was retrieved from the global hydrologic soil group and resampled to 2.5 m resolution using the nearest neighbor resampling technique to estimate the curve number

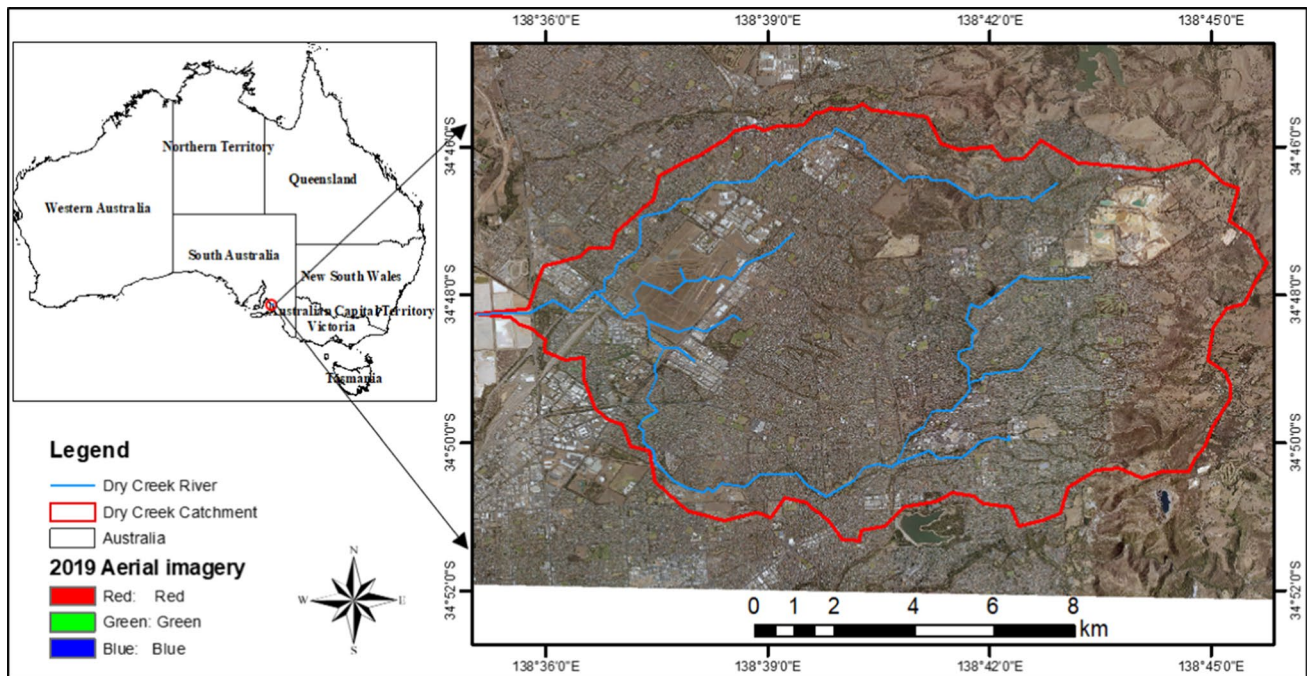


Fig. 1 Location map of dry creek catchment

Table 1 Details of the data used for this study

Data type	Date captured	Spatial resolution (m)	Spectral resolution	Source
Aerial imagery	19–27 March 1979	0.25	R, G, B	DEW
SPOT imagery	9 January 2005–16 October 2006	2.5	R, G, B, CIR	DEW
Aerial imagery	12–14 January 2019	0.075	R, G, B	DEW
Hydrologic soil group		250		ORNL DAAC
Population				ABS

*DEW = Department of Environment and Water, R = Red, G = Green, B = Blue, CIR = Color infrared, ORNL DAAC = OAK RIDGE National laboratory distributed active archive center for biogeochemical dynamics, Australian bureau of statistics

for the respective LULC class and corresponding soil (Ross et al. 2018). The nearest neighbor resampling technique was selected since it is appropriate for categorical data and does not alter the value of the input cells.

Image classification

The number of LULC classes was determined by the current condition of the catchment by visual inspection of the ground information and the imagery, the spatial and spectral resolution of the imagery, the availability of various land use practices, and the intended purpose of the classification output or the fineness of the classification. Preliminary investigations were conducted by visiting the catchment and viewing high-resolution images on Google Earth Pro. Typical land use classes in urban settings include built-up areas, vegetation, water bodies and/or wetlands, green spaces, open land, and cropland (Gashu and Gebre-Egziabher 2018; Moniruzzaman et al. 2020). By visual inspection of high-resolution imagery, four land use land cover classes (built-up, grass, water, and plantation/trees) were identified as present within the Dry Creek catchment and were thus chosen for the classification (Table 2).

The image segmentation procedure, which combines neighboring pixels that are similar in color and have geometric properties, is commonly utilized during image classification using SVM. Three criteria (spectral detail, spatial detail, and minimum segment size in pixels) govern the separation of images into objects in image segmentation. A classification schema is necessary to establish the number

and type of classes to be utilized for supervised classification. In the ArcGIS Pro 3.0 environment, a schema with four LULC classes was created and saved in an Esri classification schema file (.ecs), which employs JSON syntax (<https://pro.arcgis.com/en/pro-app/latest/help/analysis/image-analyst/the-image-classification-wizard.htm> accessed on December 15, 2022). User-defined training samples were prepared at randomly distributed locations (Fig. 2 and Table 3) for each LULC class. Object-based SVM image classification was carried out by generating 500 randomly stratified training samples per class.

Classification accuracy

The assessment of image classification accuracy helps to evaluate the precision of classification results, ensuring the reliability of subsequent analysis and applications (Foody 2008; Zhang et al. 2020). To verify the accuracy of classification, validation polygons were selected through a stratified random sampling approach, based on clearly distinguishable features observed in both aerial imagery and SPOT imagery. Five hundred randomly generated points were derived from the sampled polygon (Table 3 and Fig. 3). These points were then compared with the classified image to assess the accuracy of the classification. After evaluating the classification accuracy performance indicators, a post-classification carried out, resulting an improved classification accuracy. To assess the accuracy of classifications, a confusion matrix was generated and used to calculate the key parameters such as overall accuracy

Table 2 Description of land use land cover classes

LULC class	Description
Built-up	Residential, commercial and services, industrial, socio-economic infrastructure and mixed urban and other urban, transportation, roads and airport, and bare ground
Grass	Parks, sport fields, and backyards
Water	Rivers, ponds, and reservoirs
Plantation/trees	Trees, shrubs, and mixed forest

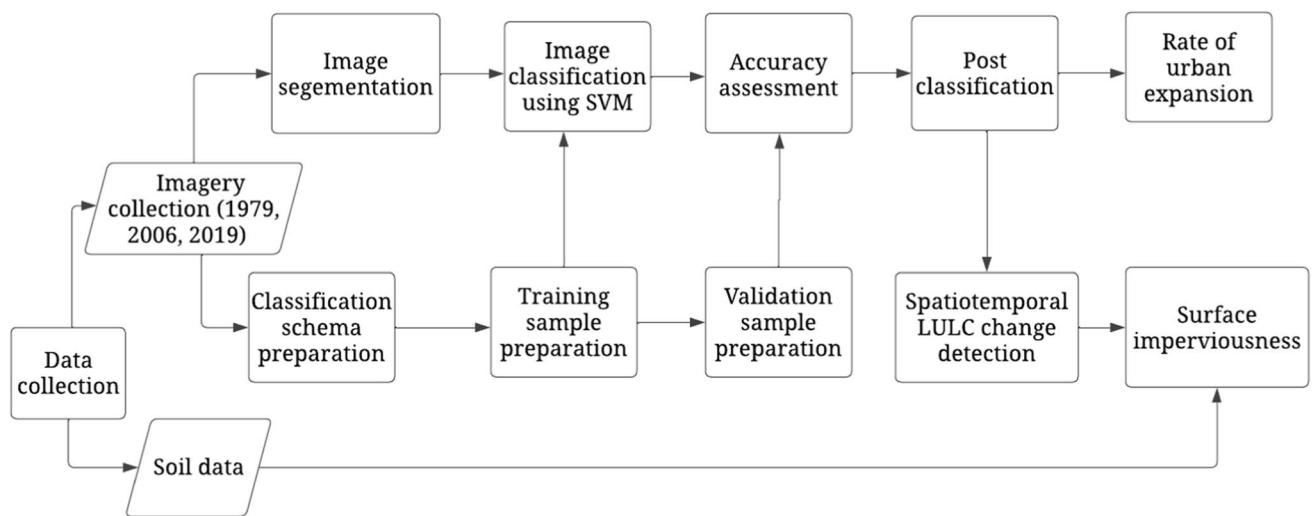


Fig. 2 Overall research framework

Table 3 Training and validation samples used for classification and accuracy assessment

LULC class	Training samples		Validation samples	
	Number of samples	Pixels (%)	Number of samples	Pixels (%)
Built-up	98	35.9	96	44.6
Grass	16	44.2	16	33.4
Plantation/trees	24	10.4	7	18.6
Water	5	9.5	3	3.3

(OA), kappa coefficient (*k*), users’ accuracy (UA), and producers’ accuracy (PA) parameters (Adelisardou et al. 2022; Shawul and Chakma 2019; Zhang et al. 2020).

The individual class accuracy was assessed using the two indices PA and UA, which were computed using Eqs. 1 and 2, respectively (Congalton and Green 2019). The former index, PA reflects the likelihood of a reference pixel being correctly classified, while the later index, UA indicates the likelihood that a pixel classified on the map depicts that category on the ground (Congalton 1991). The OA that provides a comprehensive measure of how accurately the model predicts the correct class across all classes, is computed using Eq. 3 (Liu et al. 2007). The kappa coefficient evaluates how accurately the classification performed as compared to just randomly assigning values. The kappa coefficient measures the agreement between classification and truth values (Table 4) and has a value between 0 and 1, with 1 being perfect agreement and 0 representing no agreement. The kappa analysis is a discrete multivariate approach for testing classification accuracy or agreement between classified and reference data points (Rwanga and Ndambuki 2017).

$$UA_i = \frac{n_{ii}}{n_{i+}} \tag{1}$$

$$PA_i = \frac{n_{ii}}{n_{+i}} \tag{2}$$

$$OA = \frac{\sum n_{ii}}{n} \tag{3}$$

$$\Delta = \frac{CA_n - CA_{n-1}}{CA_{n-1}} \times 100 \tag{4}$$

Change detection

Post-classification comparison was used to detect changes in LULC at three different time periods. Change detection can be either a categorical change, pixel value change, or time series change. Categorical change computes the change between two thematic rasters and quantifies and explores the pixels that are changed or remained unchanged. The pixel value change computes the absolute or relative change between the two continuous raster images. Time series change uses LandTrendr to analyze changes in a multidimensional raster and compute the date on which each pixel changed. LandTrendr uses regression—and vertex-to-vertex-based trajectory fitting to detect abrupt events, such as disturbances, as well as longer duration processes, such as regrowth (Kennedy et al. 2010). Change detection was performed using a comparative analysis of spectral classifications produced independently at times t1 and t2 (Hussien et al. 2022). The percentages of LULC change detection

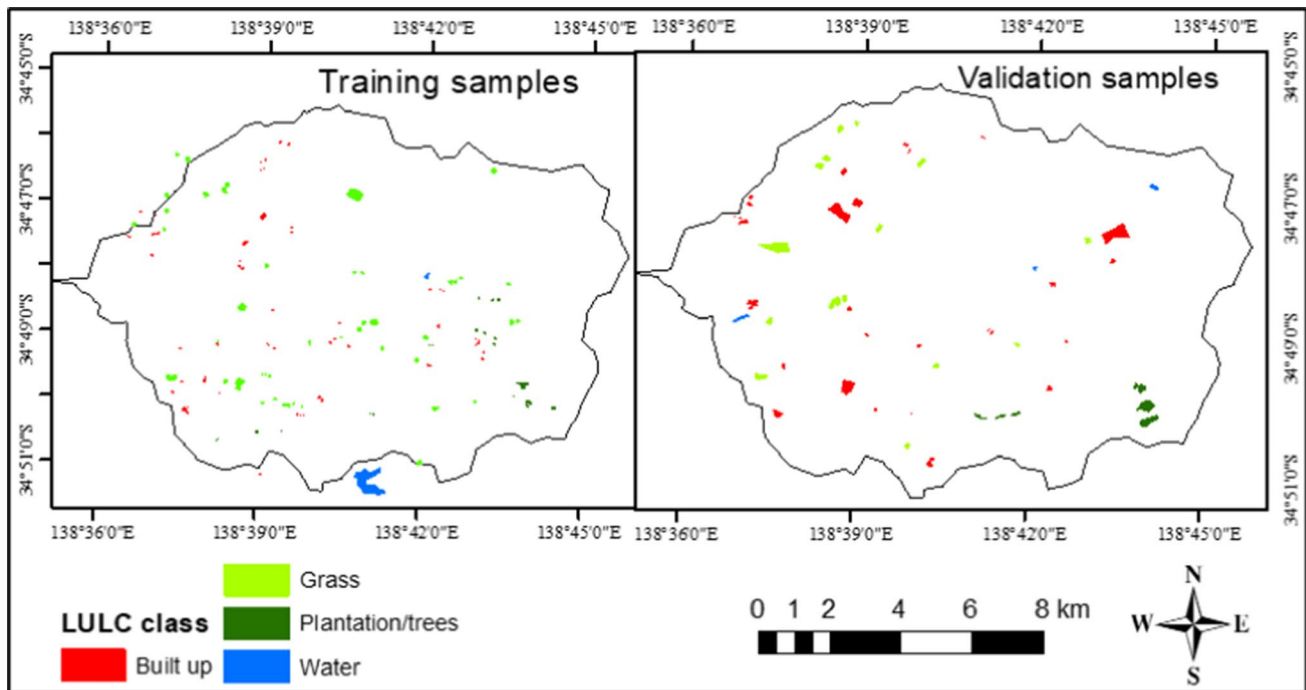


Fig. 3 Spatial distribution of training samples (left) and validation samples (right)

Table 4 Error matrix with n_{ij} representing the pixel count in the mapped land cover category i and the reference land cover category j adapted from Congalton and Green (2019)

Classified	Reference				
	1	2	3	4	Total
1	n_{11}	n_{12}	n_{13}	n_{14}	n_{1+}
2	n_{21}	n_{22}	n_{23}	n_{24}	n_{2+}
3	n_{31}	n_{32}	n_{33}	n_{34}	n_{3+}
4	n_{41}	n_{42}	n_{43}	n_{44}	n_{4+}
Total	n_{+1}	n_{+2}	n_{+3}	n_{+4}	n

n is the total pixel count

and the rate of change were estimated using Eqs. 5 and 6, respectively.

$$\Delta = \frac{CA_n - CA_{n-1}}{CA_{n-1}} * 100 \tag{5}$$

$$R_C = \frac{CA_n - CA_{n-1}}{N} \tag{6}$$

$$R_{ue} = \frac{BA_n - BA_{n-1}}{BA_{n-1} * N} * 100 \tag{7}$$

where Δ is percent change, R_C is rate of change, R_{ue} is rate of urban expansion, N is the number of years between the

two LULC maps, CA_{n-1} and CA_n are the initial and final LULC class area coverage (in km^2), BA_{n-1} and BA_n are the built-up area at time t_{n-1} and t_n (in km^2). The rate of urban sprawl/expansion between the three study periods was also determined using Eq. 7.

Impact of urbanization on surface imperviousness

Surface imperviousness is altered by urbanization; imperviousness can be evaluated in hydrological studies using the runoff coefficient, curve number, and retention capacity. In this study, built-up areas, such as buildings, parking lots, and roadways, were considered as impervious surfaces. The curve number represents the stormwater runoff capacity of a drainage basin. It is an empirical measure used in hydrology to anticipate direct runoff or infiltration from excess rainfall (Cronshey et al. 1985), and is estimated as a function of land use, soil type, and antecedent catchment moisture using the Soil Conservation Service (SCS) Technical Release 55 (TR-55) tables (SCS 1986). The ArcGIS Pro 3.0 environment was used to combine the LULC and hydrologic soil groups and apply the corresponding curve number value using the SCS TR-55 table. Equation 8 was used to calculate the composite curve number value for each year. The potential maximum retention is a measure of a watershed’s ability to extract and absorb storm precipitation and is calculated using Eq. 9 from the curve number. The runoff coefficient, which quantifies the percentage of rainwater flowing out of a certain surface during

a storm event, was assigned for each year and LULC class. Equation 10 was used to generate the weighted runoff coefficient and Eq. 11 for estimating the equivalent impervious area that are used to compute runoff utilizing the rational technique for individual LULC class.

$$CN_{\text{composite}} = \frac{\sum A_i * CN_i}{\sum A_i} \tag{8}$$

$$S = \frac{25400}{CN} - 254 \tag{9}$$

$$C_w = \frac{\sum A_i * C_i}{\sum A_i} \tag{10}$$

$$EIA = C_i \times A_i \tag{11}$$

where $CN_{\text{composite}}$ is the composite curve number used for runoff volume computations; C_w is the weighted runoff coefficient; i is an index for the catchment subdivisions of uniform land use and soil type; CN_i is the curve number for subdivision i ; C_i is runoff coefficient value for each subdivision; EIA is the equivalent impervious area (km^2), and A_i is the drainage area of subdivision i (km^2).

Results and discussion

Accuracy of LULC classification

The overall accuracy and kappa coefficient obtained from the confusion matrix agreed consistently demonstrated strong

Table 5 Classification accuracy of 1979 aerial imagery

Class name	Built-up	Grass	Plantation/trees	Water	Total	UA	kappa
Built-up	148	2	0	0	150	0.99	
Grass	14	196	6	0	216	0.91	
Plantation/trees	14	18	69	0	101	0.68	
Water	0	0	2	31	33	0.94	
Total	176	216	77	31	500		
PA	0.84	0.91	0.90	1.00		0.89*	
kappa							0.83

*Overall accuracy

Table 6 Classification accuracy of 2006 SPOT imagery

Class name	Built-up	Grass	Plantation/trees	Water	Total	UA	kappa
Built-up	144	0	0	0	144	1.00	
Grass	30	215	2	0	247	0.87	
Plantation/trees	2	1	75	0	78	0.96	
Water	0	0	0	31	31	1.00	
Total	176	216	77	31	500		
PA	0.82	1.00	0.97	1.00		0.93*	
kappa							0.89

*Overall accuracy

Table 7 Classification accuracy of 2019 aerial imagery

Class name	Built-up	Grass	Plantation/trees	Water	Total	UA	kappa
Built-up	186	0	0	0	186	1.00	
Grass	15	146	1	0	162	0.90	
Plantation/trees	22	21	92	0	135	0.68	
Water	0	0	0	17	17	1.00	
Total	223	167	93	17	500		
PA	0.83	0.87	0.98	1.00		0.88*	
kappa							0.83

*Overall accuracy

agreement, with values exceeding 0.83 for all three periods (Tables 5, 6, 7). According to McHugh (2012), classification accuracy is considered strong when the kappa values range between 0.80 and 0.90. SPOT imagery outperformed others in classification accuracy, with an overall accuracy and kappa coefficient values of 0.93 and 0.89, respectively (Table 6). This is attributed to SPOT's four spectral bands (red, green, blue, and color infrared) spectral resolution, which facilitate clear differentiation between various LULC classes. A similar study conducted in Melbourne by Jamei et al. (2022) obtained comparable kappa coefficient values of 82.3% using the random forest tree classification algorithm. Rwanga and Ndambuki (2017) also stated that the classification is regarded as almost perfect when the kappa value falls between 0.81 and 1. Similarly, Hussien et al. (2022) also found a comparable kappa value of 0.93 for the Abbay River Basin.

Spatiotemporal land use and land cover maps

The classification results revealed that in 1979, the catchment was dominated by grass cover occupying an area of 67.65 km² followed by built-up and plantation with 24.9 km² and 22.52 km² areal coverage, respectively (Table 8). By 2006, the catchment's LULC distribution shifted with

built-up and grass areas covering 45.58 km² and 41.27 km², respectively. Furthermore, in 2019, the built-up area within the catchment significantly expanded to 58.88 km² while grass cover reduced to 35.76 km². On the other hand, plantation and water features showed negligible changes over the 40-year period. Statistica (2023) also reported that Australia's urbanization rate has consistently been over 80% since the 1960s, reaching the highest rate of 86.36% in 2021 that increases the built-up area.

From the spatial map of the LULC maps, it was observed that grass was dominantly found in the eastern and central parts of the catchment in 1979. Most plantation/tree LULC classes have been found in the eastern (upper) parts of the catchment over the last four decades (Fig. 4).

Spatiotemporal changes in LULC classes

The LULC maps for 1979, 2006, and 2019 indicated a substantial trend of LULC change over the last four decades. Notably, the built-up areas expanded by 33.98 km² (29.46%) while the grass cover diminished by 43.09 km² (33.73%) between 1979 and 2019. During this period, the rate of change of grass cover changes closely corresponded to the rate of the built-up area change, with a decrement of

Table 8 LULC classification results of dry creek catchment

Land use name	1979		2006		2019	
	Area (km ²)	Percentage	Area (km ²)	Percentage	Area (km ²)	Percentage
Built-up	24.90	21.57	45.58	39.49	58.90	51.03
Grass	67.65	58.61	41.27	35.76	24.56	21.28
Plantation/trees	22.52	19.51	27.97	24.23	31.22	27.05
Water	0.35	0.30	0.60	0.52	0.75	0.65
Total	115.42	100	115.42	100	115.42	100

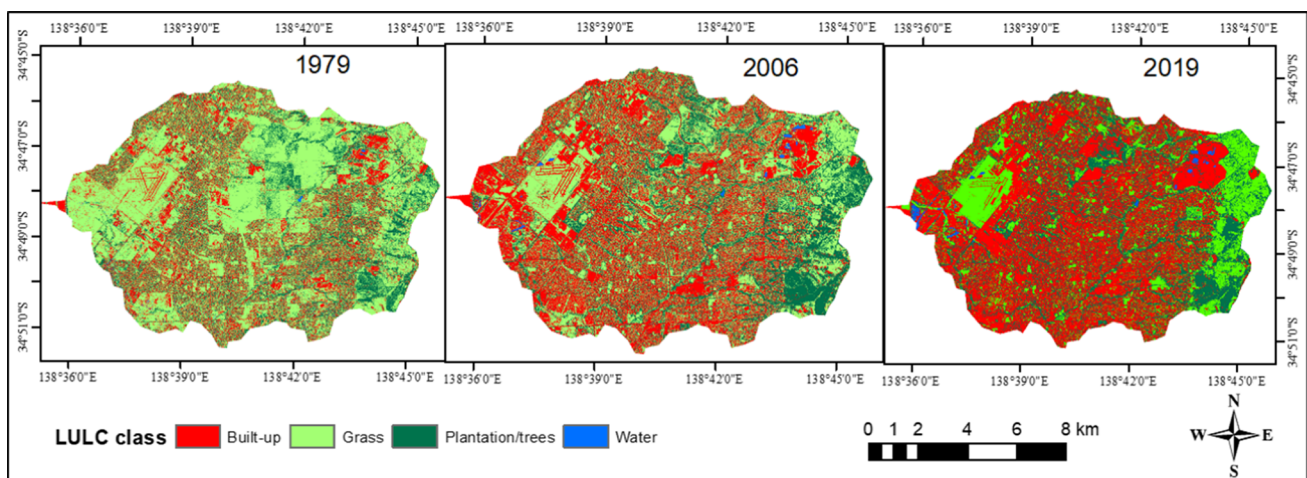
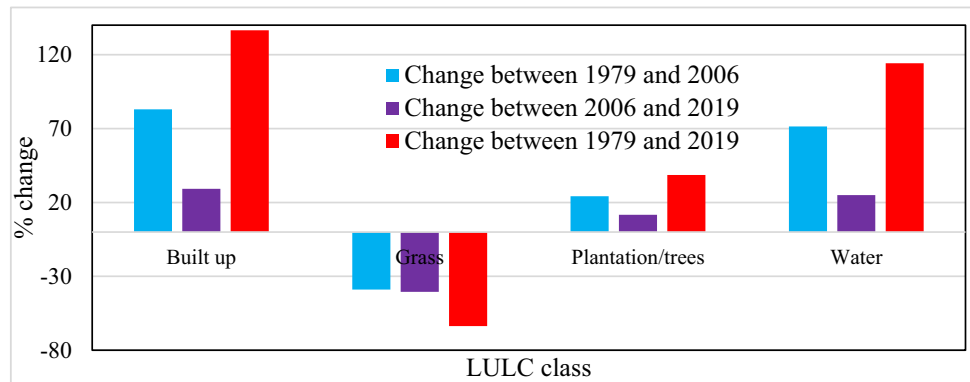


Fig. 4 Spatiotemporal distribution of LULC classes in Dry Creek catchment

Table 9 Rate of LULC change over the study period

LULC class	Change between 1979 and 2006			Change between 2006 and 2019			Change between 1979 and 2019		
	Area (km ²)	% change	Rate of change (km ² /yr)	Area (km ²)	% Change	Rate of change (km ² /yr)	Area (km ²)	% Change	Rate of change (km ² /yr)
Built-up	20.68	83.05	0.77	13.32	29.22	1.02	34.00	136.55	0.85
Grass	-26.38	-38.99	-0.98	-16.71	-40.49	-1.29	-43.09	-63.70	-1.08
Plantation/trees	5.45	24.20	0.20	3.25	11.62	0.25	8.70	38.63	0.22
Water	0.25	71.43	0.01	0.15	25.00	0.01	0.40	114.29	0.01

Fig. 5 Percentage change in each LULC class over the study period



-1.08 km²/yr for grass cover and increment of 0.85 km²/yr for built-up areas (Table 9 and Fig. 5).

In comparison with the plantation and water classes, the built-up area increased extensively. Regardless, grass cover has consistently declined over all time periods. The water class increased due to the construction of Mawson Lakes and other reservoirs in some parts of the catchment and pond water in the upstream parts of the catchment in mining holes. Between 2006 and 2019, the rate of change in built-up area was 1.03 km²/yr; whereas, the rate of change in grass cover was -1.29 km²/yr.

Plantation coverage increased due to the implementation of Urban Forest Biodiversity Program (UFBP, 2002) and urban greening, which includes private greening, streetscapes and transportation corridors, riparian vegetation or green and blue corridors, and urban parks. Riparian landscapes (lands near rivers and streams) help to stabilize stream channel morphology, protect streams from upland pollution sources, and divert sediment-producing activities away from the stream (McKergow et al. 2003).

Post-classification categorical LULC change detection was carried out in ArcGIS Pro 3.0. A significant transition from grass to built-up areas was noted due to increased population and urbanization, with strong demand for residential, commercial, and industrial buildings with car parks and roadways. There was also a visible transition from built-up area to grass cover. This was because places under development were entirely regarded as built-up areas and later

developed with backyards and some trees, particularly in residential districts.

The spatial changes in LULC and urbanization showed that the central, northeastern, and southern parts of the catchment significantly changed from grass cover to built-up areas in the three consecutive study periods (Fig. 6). This resulted in an overall increase in impervious area throughout the catchment. The plantation/trees showed a slight increase due to the conservation practices of river buffers and parks as well as an overall urban greening. The development of Mawson Lakes Pond in downstream areas and other ponds in upstream mining areas resulted in a minor increase in the spatial distribution of water features within the catchment. During the period between 1979 and 2006, approximately 55.7% of the catchment experienced distinct categorical changes in LULC distribution (Table 10). Furthermore, between 2006 and 2019, approximately 44.08% of the catchment experienced categorical shift in LULC (Table 11). Notably, over the entire study period (1979–2019), approximately 62.98% of the catchments showed categorical changes between the LULC classes (Table 12). A research conducted by Manandhar et al. (2010) in the Lower Hunter district of New South Wales also reported that approximately 28% of the study area underwent changes in land use and land cover classes.

Approximately 72.68 km² of the catchment area experienced categorical LULC changes between 1979 and 2019, with a maximum extent of 32.26 km² of grass cover

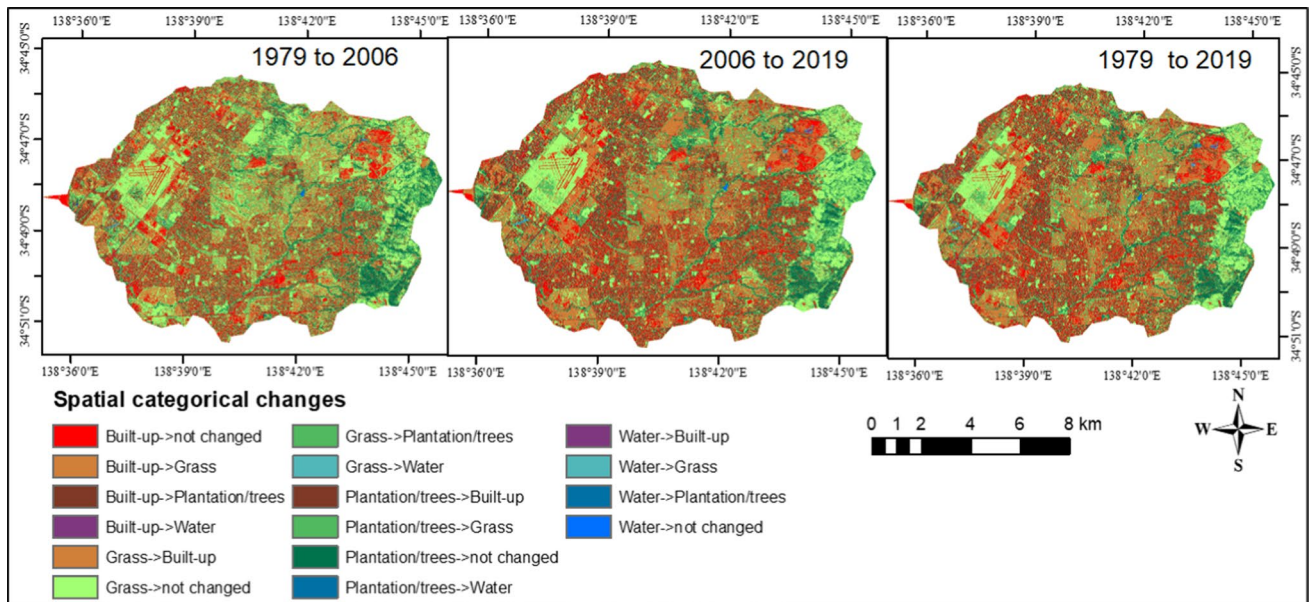


Fig. 6 Spatial categorical changes of LULC between the three study periods

Table 10 Categorical LULC changes between 1979 and 2006

Category	1979	2006	Area (km ²)	% Change
Changed	Built-up	Grass	7.19	6.23
	Built-up	Plantation/trees	3.71	3.21
	Built-up	Water	0.20	0.17
	Grass	Built-up	23.35	20.23
	Grass	Plantation/trees	15.53	13.46
	Grass	Water	0.29	0.25
	Plantation/trees	Built-up	7.71	6.68
	Plantation/trees	Grass	5.87	5.09
	Plantation/trees	Water	0.09	0.08
	Water	Built-up	0.17	0.15
	Water	Grass	0.10	0.09
	Water	Plantation/trees	0.08	0.07
	Total		64.29	55.70
Unchanged	Built-up	Built-up	14.34	12.42
	Grass	Grass	28.10	24.35
	Plantation/trees	Plantation/trees	8.66	7.50
	Water	Water	0.03	0.03
	Total		54.13	44.30

Table 11 Categorical LULC change between 2006 and 2019

Category	2006	2019	Area (km ²)	% Change
Changed	Built-up	Grass	5.34	4.63
	Built-up	Plantation/trees	6.40	5.55
	Built-up	Water	0.28	0.24
	Grass	Built-up	18.38	15.93
	Grass	Plantation/trees	8.40	7.28
	Grass	Water	0.10	0.09
	Plantation/trees	Built-up	6.67	5.78
	Plantation/trees	Grass	4.81	4.17
	Plantation/trees	Water	0.12	0.10
	Water	Built-up	0.29	0.25
	Water	Grass	0.02	0.02
	Water	Plantation/trees	0.06	0.05
	Total		50.87	44.08
Unchanged	Built-up	Built-up	33.54	29.06
	Grass	Grass	14.40	12.48
	Plantation/trees	Plantation/trees	16.36	14.18
	Water	Water	0.24	0.21
Total			64.54	55.92

Table 12 Categorical LULC change between 1979 and 2019

Category	1979	2019	Area (km ²)	% Change	
Changed	Built-up	Grass	3.60	3.12	
	Built-up	Plantation/ trees	4.66	4.04	
	Built-up	Water	0.16	0.14	
	Grass	Built-up	32.26	27.95	
	Grass	Plantation/ trees	17.58	15.23	
	Grass	Water	0.48	0.42	
	Plantation/ trees	Built-up	9.95	8.62	
	Plantation/ trees	Grass	3.61	3.13	
	Plantation/ trees	Water	0.07	0.06	
	Water	Built-up	0.18	0.16	
	Water	Grass	0.05	0.04	
	Water	Plantation/ trees	0.08	0.07	
	Total			72.68	62.98
	Unchanged	Built-up	Built-up	16.49	14.29
Grass		Grass	17.32	15.01	
Plantation/ trees		Plantation/ trees	8.89	7.70	
Water		Water	0.03	0.03	
Total			42.73	37.02	

Table 13 Urban expansion rate in dry creek catchment during the three study periods

Urban expansion	1979–2006	2006–2019	1979–2019
Expansion area (km ²)	20.6	13.32	34.00
Expansion percentage (%)	83.05	29.22	136.55
Expansion rate (km ² a ⁻¹)	0.77	1.02	0.85
Annual change rate (%)	3.08	2.25	3.41

converted to built-up. During the study period, only 37.02% of the catchment area remained unchanged (Table 12). In addition to categorical change identification, works such as Manandhar et al. (2010) employ post-classification change detection based on a transition matrix constructed with two-dimensional tables, with the rows of the matrix illustrating the initial map class and the columns representing the subsequent map categories. Jamei et al. (2022) reported similar findings in Melbourne, where population growth and urban expansion caused a notable change in LULC.

The study found that urban expansion across the entire study period was 34 km², with an average annual change rate of 3.41% specifically within the built-up area. This observation indicated that urban development in the study area has

Table 14 South Australia population growth statistics

Year	1979	2006	2016	2021
Total population growth rate	0.38	0.89	0.72	
Population	1,301,109	1,552,529	1,712,843	1,778,813

Table 15 Projected population for South Australia (SA) and inner north suburbs of Adelaide (AIN)

Year	2016	2021	2026	2031	2036
AIN	303,485	315,367	329,188	340,452	349,495
SA	865,966	898,985	935,976	971,602	1,004,613

been increasing (Table 13). In a similar study conducted by Ma and Xu (2010) in Guangzhou City, China, revealed a notably higher annual rate of change reaching 9.7% during the study period between 1995 and 2002.

Population growth and contributions to LULC

According to the Australian Bureau of Statistics (ABS), Australia’s population has increased by over 25% from 2001 to 2016, reaching twenty-four million people. Currently, 90% of Australians live in cities, which was 60% in 1911. Notably, overseas migration currently has accounted for slightly over 55% of Australia’s population growth since 2001, making it as the predominant contributor to the country’s population growth (ABS 2019). The Australian Bureau Statistics data for South Australia showed that the state’s population increased by 251,420 residents between 1979 and 2006, followed by an increase 226,284 individuals between 2006 and 2021 (Table 14).

The population statistics of inner north suburbs of Adelaide, in which Dry Creek is located, has shown consistent upward trajectory from the baseline census population in 2016 to the 2036 projection (Table 15). Between 2016 and 2021, there was a noticeable increase of 11,882 people. This rate of growth is anticipated to be maintained, with the population expected to increase by 34,128 people between 2021 and 2036 (Department of Planning Transport and Infrastructure 2019b). This projected increase in population will increase demand for the number of new residential houses and other institutional, commercial, and recreational built-up areas. The increase in population, has directly contributed to the increase in built-up area coverage in the Dry Creek catchment. This demonstrates how the need for residential buildings, parking lots, and other infrastructure has been raised by an expanding population. There was a strong correlation between the changes in LULC and population

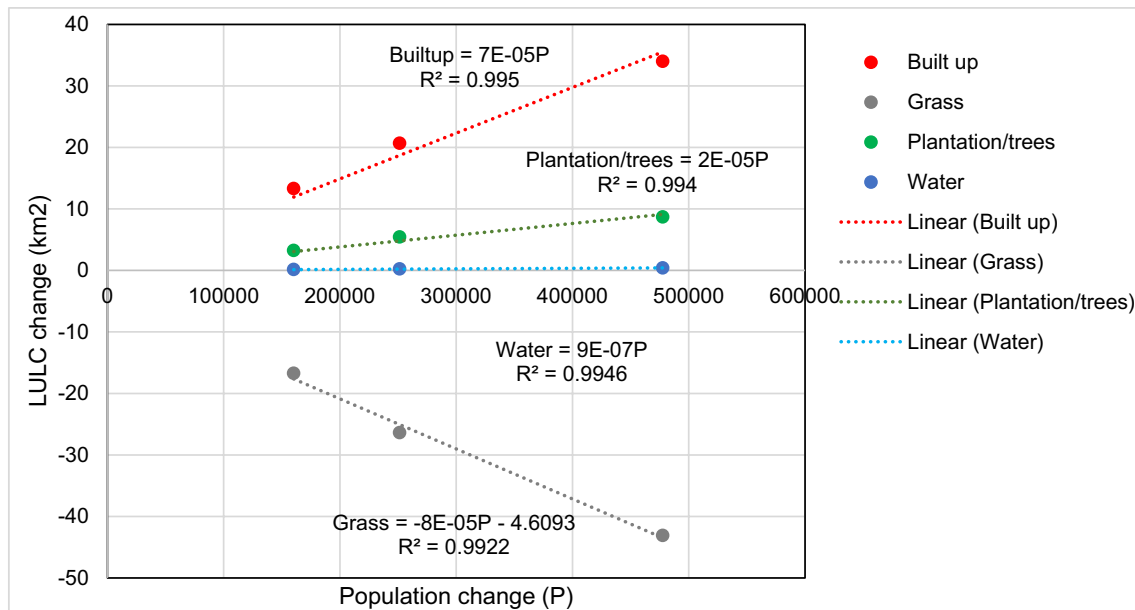


Fig. 7 Variation of LULC changes against population changes over the study period

changes. While most LULC classes showed a strong positive correlation, grass cover demonstrated a strong negative correlation (Fig. 7). Although, the amount of data available is limited in performing an in-depth quantitative analysis of the historical trends and correlation between changes in LULC and population, the trends presented using the available data reveal that ongoing population changes will continue to influence the changes in LULC across the Dry Creek catchment.

Ding et al. (2022) confirmed a similar result, with a growth in population having a substantial positive association with an increase in urban land. Similarly, Ouedraogo et al. (2010) investigated the significant relationship between the population and areas of cropland and open woodland in Burkina Faso. From the projected population, it was observed that the population will continue to increase impacting the current LULC, which further impacts the hydrology of the catchment.

Urbanization impact on catchment surface imperviousness

The surface imperviousness of a catchment is highly inter-related to the runoff coefficient and runoff generation capacity (Feng et al. 2021). In the Dry Creek catchment, significant urbanization has increased the built-up areas. Surface imperviousness is significantly correlated with built-up areas in the catchment. Built-up areas were classified as impermeable surfaces; whereas, water, grass, and plantation cover were classified as pervious. The analysis of the Dry Creek catchment revealed a marked 136.55% rise in

Table 16 Surface imperviousness, runoff coefficient and retention capacity of dry creek catchment

Year	1979	2006	2019	% Change between 1979 and 2019
Pervious area (km ²)	90.52	69.84	56.52	-37.56
Impervious area (km ²)	24.90	45.58	58.90	136.55
EIA (km ²)	38.34	52.44	61.58	60.63
Weighted runoff coefficient	0.33	0.46	0.53	60.63
Weighted curve number	80.94	84.87	87.37	7.95
Retention capacity at AMCII	59.83	45.26	36.76	-38.56

* AMC II indicates the antecedent moisture condition II, (-) indicates a decrease in the parameter over the study period

imperviousness, with corresponding 37.56% decrease in pervious areas (Table 16). This suggests that the conversion of other LULC classes to built-up classes as a result of urbanization contributes to surface imperviousness (Shuster et al. 2005). An increasing trend of urbanization across the catchment makes a direct influence on the runoff coefficient and equivalent impervious area (Fig. 8 and Table 16). A noticeable spatial change in the runoff coefficient and equivalent impervious area are particularly significant in the central, northern, and western parts of the catchment. The increase in the runoff coefficient and equivalent impervious area increases the volume of runoff generated from the catchment by reducing infiltration of water into the underlying soil layer thus impacting groundwater recharge. Runoff also occurs more rapidly from impervious areas than runoff from pervious areas—hence flooding downstream. The weighted

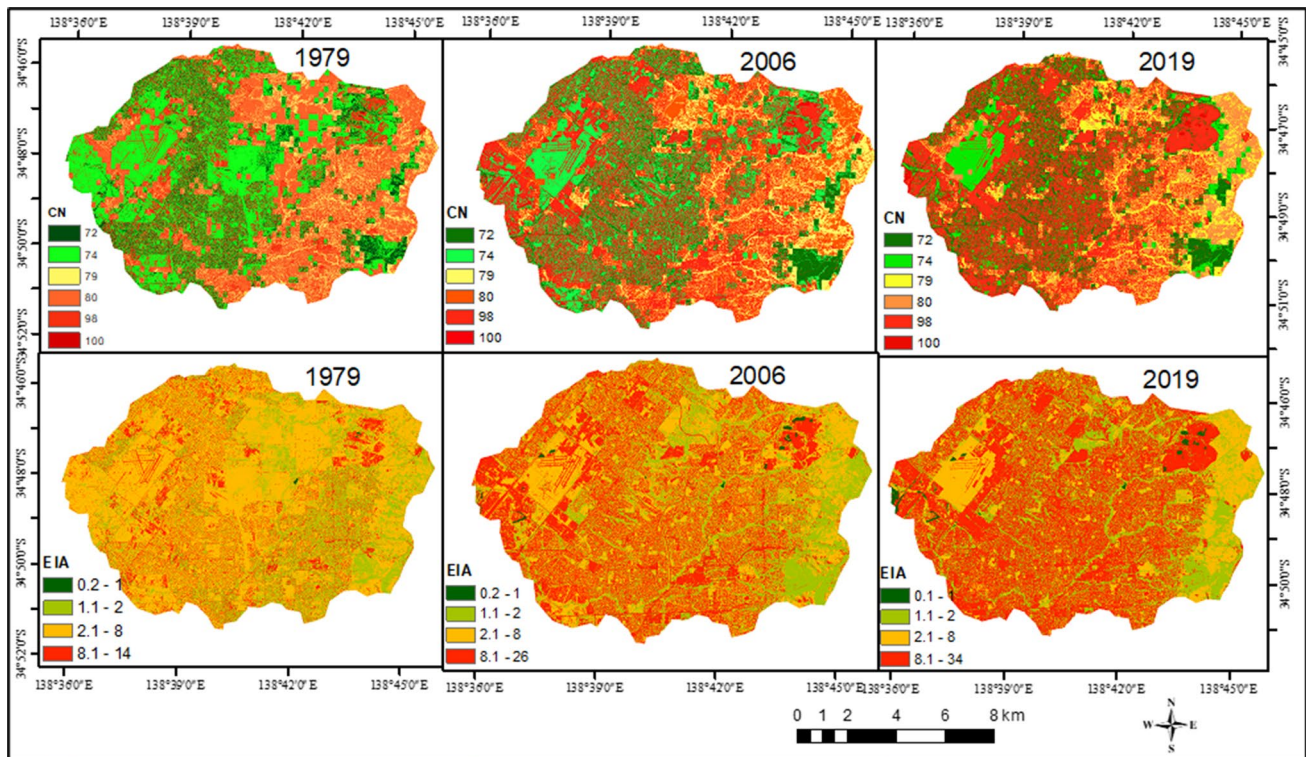


Fig. 8 Spatiotemporal distribution of curve number and EIA within Dry Creek catchment

runoff coefficient of the Dry Creek catchment increased from 0.33 to 0.53 while EIA from 38.34 to 61.58 km², increasing the volume of runoff estimated using the rational method. Greater runoff volume increases the risk of flooding in downstream sections of the catchment. A study conducted on the effects of urbanization on storm runoff in Kathmandu city by Bajracharya et al. (2015) also showed that urbanization increases the surface imperviousness and runoff volume. Similarly, a study by Zhang et al. (2015) in Madagascar found an increase in urbanized area by 52%, runoff depth by 58% and runoff coefficient by 5.8%. Further, the study by McMahon et al. (2003) emphasized that the assessment of extreme low and high-flow episodes’ frequency, magnitude, and duration should consider the impervious surface area’s contribution to streamflow generation processes.

Irrespective of the rainfall condition, the catchment’s weighted curve number exhibited an increase from 80.94 to 87.37 (Table 16). Ansari et al. (2016) also observed the increase in built-up areas in Nagpur urban watershed in India raised the magnitude of curve number from 76 to 80 between 2000 and 2012. The increase in the curve number resulted in a 38.56% decline in retention capacity and increasing the risk of flooding to the surrounding environment. The hydrological cycle is fundamentally affected by the type of soil and land cover because it regulates infiltration and affects surface and groundwater fluxes (Jaafar et al. 2019; Malede

et al. 2023). Overall, changes in LULC due to urbanization in Dry Creek alter the surface imperviousness, runoff coefficient, equivalent impervious area, curve number, and retention capacity of the soil, which could potentially have an impact on the hydrological conditions of the catchment, including runoff and groundwater recharge.

Conclusion

The study of LULC change caused by urbanization is crucial for analyzing the influence of urban sprawl on catchment surface imperviousness and its consequences for the hydrological processes of urban catchments. High-quality data and a reliable classification method using remote sensing are helpful in the study of changes in land use land cover. LULC classification utilizing high-quality images provide more accurate classification results, which can subsequently be used for environmental and hydrological studies. In the present study, very high-resolution aerial imagery with a resolution of 0.075 m and SPOT satellite imagery with a resolution of 2.5 m were utilized to assess the long-term spatiotemporal LULC changes caused by urban sprawl over the Dry Creek catchment. This study developed LULC maps of the area and assessed categorical changes in the catchment using an advanced

and user-friendly ArcGIS Pro 3.0 environment employing the SVM method of image classification. Following an examination of the accuracy assessment performance indicators of automatic classification, image post-classification was demonstrated to improve the classification accuracy. The overall classification accuracy was found to be high, with kappa coefficient and overall accuracy results greater than 0.83 and 0.88, respectively. The SVM image classification approaches performed well in classifying high-resolution imageries, with good performance metrics. The built-up area, plantation and water expanded by 34.0 km², 8.7 km² and 0.4 km², respectively from 1979 to 2019, whereas grass cover declined by 43.09 km², revealing a significant transformation in the LULC. Between 1979 and 2019, the study area has undergone substantial changes in land use and land cover. The LULC in the study area changed categorically by 62.98% during the study period. High rates of change were observed in the grass and built-up areas, with respective values of −1.08 and 0.85 km²/yr. Urbanization raised the impervious surface from 24.90 to 58.90 km² with 136.55% urban expansion. During the study period, an increase in surface imperviousness increased the runoff coefficient and curve number by 60.63% and 7.95%, respectively, while decreasing soil retention capacity by 38.56%. This undoubtedly increases the quantity of catchment surface runoff by increasing the risk of flooding to the downstream environment. The findings of this study have significant implications for the development and implementation of flood and stormwater control strategies. Therefore, future research should focus on how LULC changes caused by urbanization affect runoff and other hydrological and morphological catchment parameters.

Acknowledgements The authors acknowledge the University of South Australia and the Australian government for providing fund to support this research. The authors also appreciate South Australia, Department of Environment and Water for providing high-resolution aerial imagery and SPOT satellite imagery.

Author contributions TGA contributed to conceptualization, methodology, software, validation, formal analysis, investigation, and writing—original draft preparation; SP contributed to software, methodology; review and editing, and supervision; GH contributed to conceptualization, review and editing, and supervision; BM contributed to review and editing, and supervision; and JB contributed to review and editing and supervision. All the authors have read and agreed to the published version of the manuscript.

Funding This research is supported by the Commonwealth of Australian Government Research Training Program (RTP).

Data availability The data can be provided up on required approval of the UniSA-STEM and SA-DEW. If interested in the data used in this research work, please contact https://andtg003@mymail.unisa.edu.au.

Declarations

Conflict of interest All the authors of this manuscript declare that this work is original and not published. There is no competing interest between authors.

Open Access This article is licensed under a Creative Commons Attribution 4.0 International License, which permits use, sharing, adaptation, distribution and reproduction in any medium or format, as long as you give appropriate credit to the original author(s) and the source, provide a link to the Creative Commons licence, and indicate if changes were made. The images or other third party material in this article are included in the article's Creative Commons licence, unless indicated otherwise in a credit line to the material. If material is not included in the article's Creative Commons licence and your intended use is not permitted by statutory regulation or exceeds the permitted use, you will need to obtain permission directly from the copyright holder. To view a copy of this licence, visit <http://creativecommons.org/licenses/by/4.0/>.

References

- ABS (2019) Australian historical population statistics.
- Aburas MM, Ahamad MSS, Omar NQ (2019) Spatio-temporal simulation and prediction of land-use change using conventional and machine learning models: a review. *Environ Monit Assess* 191(4):1–28
- Adelisaridou F, Zhao W, Chow R, Mederly P, Minkina T, Schou J (2022) Spatiotemporal change detection of carbon storage and sequestration in an arid ecosystem by integrating google earth engine and InVEST (the Jiroft plain, Iran). *Int J Environ Sci Technol* 19(7):5929–5944
- Amani M, Salehi B, Mahdavi S, Brisco B (2018) Spectral analysis of wetlands using multi-source optical satellite imagery. *ISPRS J Photogramm Remote Sens* 144:119–136
- Ansari TA, Katpatal YB, Vasudeo A (2016) Spatial evaluation of impacts of increase in impervious surface area on SCS-CN and runoff in Nagpur urban watersheds. *India Arab J Geosci* 9(18):1–15
- Bajracharya AR, Rai RR, Rana S (2015) Effects of urbanization on storm water run-off: a case study of Kathmandu Metropolitan City. *Nepal J Inst Eng* 11(1):36–49
- Basheer S, Wang X, Farooque AA, Nawaz RA, Liu K, Adekanmbi T, Liu S (2022) Comparison of land use land cover classifiers using different satellite imagery and machine learning techniques. *Remote Sens* 14(19):4978
- Blaschke T, Hay GJ, Kelly M, Lang S, Hofmann P, Addink E, Feitosa RQ, Van der Meer F, Van der Werff H, Van Coillie F (2014) Geographic object-based image analysis—towards a new paradigm. *ISPRS J Photogramm Remote Sens* 87:180–191
- Bledsoe BP (2002). Relationships of stream responses to hydrologic changes. Linking stormwater BMP designs and performance to receiving water impact mitigation
- Chandra MA, Bedi S (2021) Survey on SVM and their application in image classification. *Int J Inf Technol* 13(5):1–11
- Chen D, Stow D, Gong P (2004) Examining the effect of spatial resolution and texture window size on classification accuracy: an urban environment case. *Int J Remote Sens* 25(11):2177–2192
- Chin A, O'dowd A, Gregory K (2013) 9.39 urbanization and river channels. *Treat Geomorphol* 1:809–827
- Ciupa T, Suligowski R (2020) Impact of the city on the rapid increase in the runoff and transport of suspended and dissolved solids during rainfall—the example of the silnica river (Kielce, Poland). *Water (Switzerland)* 12(10):2693. <https://doi.org/10.3390/w12102693>

- Clark R, Gonzalez D, Dillon P, Charles S, Cresswell D, Naumann B (2015) Reliability of water supply from stormwater harvesting and managed aquifer recharge with a brackish aquifer in an urbanising catchment and changing climate. *Environ Model Softw* 72:117–125
- Congalton RG (1991) A review of assessing the accuracy of classifications of remotely sensed data. *Remote Sens Environ* 37(1):35–46
- Congalton RG, Green K (2019) Assessing the accuracy of remotely sensed data: principles and practices. CRC Press
- Cronshey R, Roberts R, Miller N (1985) Urban hydrology for small watersheds (TR-55 Rev). Hydraulics and hydrology in the small computer age
- Dabija A, Kluczek M, Zagajewski B, Raczek E, Kycko M, Al-Sultani AH, Tardà A, Pineda L, Corbera J (2021) Comparison of support vector machines and random forests for corine land cover mapping. *Remote Sens* 13(4):777
- Demeke G, Andualem T (2018) Application of remote sensing for evaluation of land use change responses on hydrology of Muga watershed, Abbay River Basin. *Ethiopia J Earth Sci Clim Change* 9(493):2
- Department of Planning Transport and Infrastructure (2019a) Population projections for South Australia Statistical local areas, 2016–36, December 2019 release.
- Department of Planning Transport and Infrastructure (2019b) Population projections for south australian statistical local areas, 2016–36, December 2019 release.
- Ding K, Huang Y, Wang C, Li Q, Yang C, Fang X, Tao M, Xie R, Dai M (2022) Time series analysis of land cover change using remotely sensed and multisource urban data based on machine learning: a case study of Shenzhen, China from 1979 to 2022. *Remote Sens* 14(22):5706
- Feng B, Zhang Y, Bourke R (2021) Urbanization impacts on flood risks based on urban growth data and coupled flood models. *Nat Hazards* 106(1):613–627
- Fisher JR, Acosta EA, Dennedy-Frank PJ, Kroeger T, Boucher TM (2018) Impact of satellite imagery spatial resolution on land use classification accuracy and modeled water quality. *Remote Sens Ecol Conserv* 4(2):137–149
- Foody GM (2008) Harshness in image classification accuracy assessment. *Int J Remote Sens* 29(11):3137–3158
- Gashu K, Gebre-Egziabher T (2018) Spatiotemporal trends of urban land use/land cover and green infrastructure change in two Ethiopian cities: Bahir dar and hawassa. *Environ Syst Res* 7(1):1–15
- Grigorescu I, Kucsicsa G, Popovici E-A, Mitrică B, Mocanu I, Dumitrașcu M (2021) Modelling land use/cover change to assess future urban sprawl in Romania. *Geocarto Int* 36(7):721–739
- Hu Y, Dong Y (2018) An automatic approach for land-change detection and land updates based on integrated NDVI timing analysis and the CVAPS method with GEE support. *ISPRS J Photogramm Remote Sens* 146:347–359
- Hussien K, Kebede A, Mekuriaw A, Asfaw Beza S, Haile Erena S (2022) Modelling spatiotemporal trends of land use land cover dynamics in the abbay river basin Ethiopia. *Model Earth Syst Environ* 9:347
- Jaafar HH, Ahmad FA, El Beyrouthy N (2019) GCN250, new global gridded curve numbers for hydrologic modeling and design. *Sci Data* 6(1):1–9
- Jamali AA, Kalkhajeh RG, Randhir TO, He S (2022) Modeling relationship between land surface temperature anomaly and environmental factors using GEE and Giovanni. *J Environ Manag* 302:113970
- Jamei Y, Seyedmehmoudian M, Jamei E, Horan B, Mekhilef S, Stojcevski A (2022) Investigating the relationship between land use/land cover change and land surface temperature using google earth engine; case study: melbourne. *Australia Sustain* 14(22):14868
- Jat MK, Garg PK, Khare D (2008) Monitoring and modelling of urban sprawl using remote sensing and GIS techniques. *Int J Appl Earth Obs Geoinf* 10(1):26–43. <https://doi.org/10.1016/j.jag.2007.04.002>
- Kennedy RE, Yang Z, Cohen WB (2010) Detecting trends in forest disturbance and recovery using yearly Landsat time series: 1. LandTrendr—Temporal segmentation algorithms. *Remote Sens Environ* 114(12):2897–2910
- Kesikoglu MH, Atasever UH, Dadaser-Celik F, Ozkan C (2019) Performance of ANN, SVM and MLH techniques for land use/cover change detection at Sultan Marshes wetland. *Turkey Water Sci Technol* 80(3):466–477
- Lamine S, Petropoulos GP, Singh SK, Szabó S, Bachari NEI, Srivastava PK, Suman S (2018) Quantifying land use/land cover spatio-temporal landscape pattern dynamics from Hyperion using SVMs classifier and FRAGSTATS®. *Geocarto Int* 33(8):862–878
- Li X, Shao G (2014) Object-based land-cover mapping with high resolution aerial photography at a county scale in midwestern USA. *Remote Sens* 6(11):11372–11390
- Li C, Liu M, Hu Y, Shi T, Qu X, Walter MT (2018) Effects of urbanization on direct runoff characteristics in urban functional zones. *Sci Total Environ* 643:301–311
- Liu C, Frazier P, Kumar L (2007) Comparative assessment of the measures of thematic classification accuracy. *Remote Sens Environ* 107(4):606–616
- Ma Y, Xu R (2010) Remote sensing monitoring and driving force analysis of urban expansion in Guangzhou City. *China Habitat Int* 34(2):228–235
- Malede DA, Alamirew T, Kosgie JR, Andualem TG (2022) Analysis of land use/land cover change trends over birr river Watershed, Abbay Basin Ethiopia. *Environ Sustain Indic* 17:100222
- Malede DA, Alamirew T, Andualem TG (2023) Integrated and individual impacts of land use land cover and climate changes on hydrological flows over birr river watershed, Abbay Basin. *Ethiopia Water* 15(1):166
- Manandhar R, Odeh IO, Pontius RG Jr (2010) Analysis of twenty years of categorical land transitions in the lower hunter of new South Wales, Australia. *Agr Ecosyst Environ* 135(4):336–346
- Mansour S, Al-Belushi M, Al-Awadhi T (2020) Monitoring land use and land cover changes in the mountainous cities of Oman using GIS and CA-Markov modelling techniques. *Land Use Policy* 91:104414
- McHugh ML (2012) Interrater reliability: the kappa statistic. *Biochemia Medica* 22(3):276–282
- McKergow LA, Weaver DM, Prosser IP, Grayson RB, Reed AE (2003) Before and after riparian management: sediment and nutrient exports from a small agricultural catchment, Western Australia. *J Hydrol* 270(3–4):253–272
- McMahon G, Bales JD, Coles JF, Giddings EM, Zappia H (2003) Use of stage data to characterize hydrologic conditions in an urbanizing environment 1. *JAWRA J Am Water Res Assoc* 39(6):1529–1546
- Mohammed MN, Sulaiman N (2012) Intrusion detection system based on SVM for WLAN. *Procedia Technol* 1:313–317
- Moniruzzaman M, Thakur PK, Kumar P, Ashraf Al Alam M, Garg V, Rousta I, Olafsson H (2020) Decadal urban land use/land cover changes and its impact on surface runoff potential for the Dhaka City and surroundings using remote sensing. *Remote Sens* 13(1):83
- Myers B, Sapdhare H, Reeve P, Teasdale P, Mosley L, Fernandes M, Fallowfield H (2021) A decision framework for selecting stormwater management interventions to reduce fine sediments and improve coastal water quality. *Goyder Inst Water Res Tech Report Series* (21/01).

- Nguyen, L. B. (2020). Land cover change detection in northwestern Vietnam using Landsat images and google earth engine. *J Water Land Develop*
- O'Driscoll M, Clinton S, Jefferson A, Manda A, McMillan S (2010) Urbanization effects on watershed hydrology and in-stream processes in the southern United States. *Water* 2(3):605–648
- Ouedraogo I, Tigabu M, Savadogo P, Compaoré H, Odén P, Ouadba J (2010) Land cover change and its relation with population dynamics in Burkina Faso. *West Africa Land Degradat Develop* 21(5):453–462
- Peña JM, Gutiérrez PA, Hervás-Martínez C, Six J, Plant RE, López-Granados F (2014) Object-based image classification of summer crops with machine learning methods. *Remote Sens* 6(6):5019–5041
- Pradhan B (2017) *Spatial modeling and assessment of urban form*. Springer, Cham
- Rojas C, Mauricio V, Sergio O, Peters S, Constanza V (2013) Pre and post earthquake land use and land cover identification in Concepción. In: *earth observation of global changes (EOGC)*. Springer. pp 223–231 [Record #1696 is using a reference type undefined in this output style.]
- Rwanga SS, Ndambuki JM (2017) Accuracy assessment of land use/land cover classification using remote sensing and GIS. *Int J Geosci* 8(04):611
- SCS (1986) *Urban hydrology for small watersheds*, technical release no. 55 (TR-55). US Department of Agriculture, US Government Printing Office, Washington, DC.
- Shawul AA, Chakma S (2019) Spatiotemporal detection of land use/land cover change in the large basin using integrated approaches of remote sensing and GIS in the upper awash basin. *Ethiop Environ Earth Sci* 78(5):1–13
- Shuster WD, Bonta J, Thurston H, Warnemuende E, Smith D (2005) Impacts of impervious surface on watershed hydrology: a review. *Urban Water J* 2(4):263–275
- Sidhu N, Pebesma E, Câmara G (2018) Using google earth engine to detect land cover change: Singapore as a use case. *Europ J Remote Sens* 51(1):486–500
- Silva JS, da Silva RM, Santos CAG (2018) Spatiotemporal impact of land use/land cover changes on urban heat islands: a case study of Paço do Lumiar, Brazil. *Build Environ* 136:279–292
- Statistica (2023) *Degree of urbanization in Australia 2021*. Thanh Noi P, Kappas M (2017) Comparison of random forest, k-nearest neighbor, and support vector machine classifiers for land cover classification using Sentinel-2 imagery. *Sensors* 18(1):18
- Department of Planning Transport and Infrastructure (2017) *The 30-year plan for greater adelaide*.
- The Goyder Institute for Water Research. (2016) *Northern adelaide plains water stocktake technical report, the goyder institute for water research, Adelaide, South Australia*. [Record #1999 is using a reference type undefined in this output style.]
- Wilkinson J (2005) *Reconstruction of historical stormwater flows in the adelaide metropolitan area*. ACWS technical report no. 10 prepared for the adelaide coastal waters study steering committee 2005.
- Xie G, Niculescu S (2021) Mapping and monitoring of land cover/land use (LCLU) changes in the crozon peninsula (Brittany, France) from 2007 to 2018 by machine learning algorithms (support vector machine, random forest, and convolutional neural network) and by post-classification comparison (PCC). *Remote Sens* 13(19):3899
- Yin H, Pflugmacher D, Kennedy RE, Sulla-Menashe D, Hostert P (2014) Mapping annual land use and land cover changes using MODIS time series. *IEEE J Select Topics Appl Earth Observ Remote Sens* 7(8):3421–3427
- Zhang H, Chen Y, Zhou J (2015) Assessing the long-term impact of urbanization on run-off using a remote-sensing-supported hydrological model. *Int J Remote Sens* 36(21):5336–5352
- Zhang M, Huang H, Li Z, Hackman KO, Liu C, Andriamiarisoa RL, Ny Aina NRT, Li Y, Gong P (2020) Automatic high-resolution land cover production in madagascar using sentinel-2 time series, tile-based image classification and google earth engine. *Remote Sens* 12(21):3663
- Zhen Z, Quackenbush LJ, Stehman SV, Zhang L (2013) Impact of training and validation sample selection on classification accuracy and accuracy assessment when using reference polygons in object-based classification. *Int J Remote Sens* 34(19):6914–6930

Publisher's Note Springer Nature remains neutral with regard to jurisdictional claims in published maps and institutional affiliations.